THE ASTROPHYSICAL JOURNAL, 491:436–450, 1997 December 20
© 1997. The American Astronomical Society. All rights reserved. Printed in U.S.A.

MACHO ALERT 95-30: FIRST REAL-TIME OBSERVATION OF EXTENDED SOURCE EFFECTS IN GRAVITATIONAL MICROLENSING

C. ALCOCK,[1,2] W. H. ALLEN,[3] R. A. ALLSMAN,[4] D. ALVES,[1,5,6] T. S. AXELROD,[7] T. S. BANKS,[8] S. F. BEAULIEU,[9] A. C. BECKER,[2,10] R. H. BECKER,[1,5] D. P. BENNETT,[1,2,11] I. A. BOND,[12] B. S. CARTER,[3] K. H. COOK,[1,2] R. J. DODD,[3] K. C. FREEMAN,[7] M. D. GREGG,[1,5] K. GRIEST,[2,13] J. B. HEARNSHAW,[14] A. HELLER,[15] M. HONDA,[16] J. JUGAKU,[17] S. KABE,[18] S. KASPI,[15] P. M., KILMARTIN,[14,19] A. KITAMURA,[12] O. KOVO,[15] M. J. LEHNER,[2,13] T. E. LOVE,[14,19] D. MAOZ,[15] S. L. MARSHALL,[1] Y. MATSUBARA,[12] D. MINNITI,[1] M. MIYAMOTO,[20] J. A. MORSE,[21] Y. MURAKI,[12] T. NAKAMURA,[22] B. A. PETERSON,[7] M. M. PHILLIPS,[23] M. R. PRATT,[2,10,24] P. J. QUINN,[25] I. N. REID,[26] M. REID,[8] D. REISS,[10] A. RETTER,[15] A. W. RODGERS,[7] W. L. W. SARGENT,[26] H. SATO,[22] M. SEKIGUCHI,[20] P. B. STETSON,[27] C. W. STUBBS,[2,7,10,24] D. J. SULLIVAN,[8] W. SUTHERLAND,[28] A. TOMANEY,[10] T. VANDEHEI,[13] Y. WATASE,[18] D. L. WELCH,[29] T. YANAGISAWA,[12] M. YOSHIZAWA,[22] AND P. C. M. YOCK[19]
(THE MACHO AND GMAN COLLABORATIONS)
Received 1997 February 24; accepted 1997 June 26

ABSTRACT

We present analysis of MACHO Alert 95-30, a dramatic gravitational microlensing event toward the Galactic bulge whose peak magnification departs significantly from the standard point-source microlensing model. Alert 95-30 was observed in real time by the Global Microlensing Alert Network (GMAN), which obtained densely sampled photometric and spectroscopic data throughout the event. We interpret the light-curve "fine structure" as indicating transit of the lens across the extended face of the source star. This signifies resolution of a star several kiloparsecs distant.

We find a lens angular impact parameter $\theta_{\rm min}/\theta_{\rm source} = 0.715 \pm 0.003$. This information, along with the radius and distance of the source, provides an additional constraint on the lensing system. Spectroscopic and photometric data indicate the source is a M4 III star of radius $61 \pm 12\ R_\odot$, located on the far side of the bulge at $\sim$9 kpc. We derive a lens angular velocity, relative to the source, of 21.5 ± 2.9 km s^{-1} kpc^{-1}, where the error is dominated by uncertainty in the angular size of the source star. Likelihood analysis yields a median lens mass of $0.67^{+2.53}_{-0.46}\ M_\odot$, located with 80% probability in the Galactic bulge at a distance of $6.93^{+1.56}_{-2.25}$ kpc. If the lens is a main-sequence star, we can include constraints on the lens luminosity. This modifies our estimates to $M_{\rm lens} = 0.53^{+0.52}_{-0.35}\ M_\odot$ and $D_{\rm lens} = 6.57^{+0.99}_{-2.25}$ kpc.

Spectra taken during the event show that the absorption-line equivalent widths of Hα and the TiO bands near 6700 Å vary, as predicted for microlensing of an extended source. This is most likely due to center-to-limb variation in the stellar spectral lines. The observed spectral changes further support our microlensing interpretation. These data demonstrate the feasibility of using microlensing limb crossings as a tool to probe stellar atmospheres directly.

Subject headings: gravitational lensing — stars: fundamental parameters — stars: late-type

[1] Lawrence Livermore National Laboratory, Livermore, CA 94550.
[2] Center for Particle Astrophysics, University of California, Berkeley, CA 94720.
[3] Carter National Observatory, Wellington, New Zealand.
[4] Supercomputing Facility, Australian National University, Canberra, ACT 0200, Australia.
[5] Department of Physics, University of California, Davis, CA 95616.
[6] Visiting Astronomer, Cerro Tololo Inter-American Observatory.
[7] Mount Stromlo and Siding Spring Observatories, Australian National University, Weston, ACT 2611, Australia.
[8] Department of Physics, Victoria University, Wellington, New Zealand.
[9] Space Telescope Science Institute, 3700 San Martin Drive, Baltimore, MD 21218.
[10] Departments of Astronomy and Physics, University of Washington, Seattle, WA 98195.
[11] Department of Physics, University of Notre Dame, IN 46556.
[12] Solar-Terrestrial Environment Laboratory, Nagoya University, Nagoya 464-01, Japan.
[13] Department of Physics, University of California, San Diego, CA 92093.
[14] Department of Physics and Astronomy, University of Canterbury, Christchurch, New Zealand.
[15] School of Physics and Astronomy and Wise Observatory, Tel-Aviv University, Tel Aviv 69978, Israel.
[16] Institute for Cosmic Ray Research, University of Tokyo, Tokyo 188, Japan.
[17] Research Institute of Civilization, Tokai University, Hiratsuka 259-12, Japan.
[18] National Laboratory of High Energy Physics (KEK), Tsukuba 305, Japan.
[19] Faculty of Science, University of Auckland, Auckland, New Zealand.
[20] National Astronomical Observatory, Mitaka, Tokyo 181, Japan.
[21] Center for Astrophysics and Space Astronomy, University of Colorado, Campus Box 389, Boulder, CO 80309.
[22] Department of Physics, Kyoto University, Kyoto 606, Japan.
[23] Cerro Tololo Inter-American Observatory, Casilla 603, La Serena, Chile.
[24] Department of Physics, University of California, Santa Barbara, CA 93106.
[25] European Southern Observatory, Karl-Schwarzschild-Strasse 2, D-85748, Garching, Germany.
[26] Astronomy Department 105-24, California Institute of Technology, Pasadena, CA 91125.
[27] Dominion Astrophysical Observatory, 5071 West Saanich Road, RR 5, Victoria, BC V8X 4M6, Canada.
[28] Department of Physics, University of Oxford, Oxford OX1 3RH, UK.
[29] Visiting Astronomer, Cerro Tololo Inter-American Observatory.
[30] Current Information on the MACHO Collaboration's Alert events is maintained at their World Wide Web site.

1. INTRODUCTION

The MACHO Collaboration is undertaking an extensive search for gravitational microlensing by objects in the Galactic halo, bulge, and disk. Nightly observations of millions of stars in the Large Magellanic Cloud (LMC) and Galactic bulge have yielded a total of eight LMC (Alcock et al. 1998) and more than 120 bulge events (Alcock et al. 1995a; Alcock et al. 1997; MACHO Alert system[30]). Similar observations are being undertaken toward the LMC by EROS (Ansari et al. 1996) with two reported events, as well as toward the bulge by OGLE (Paczyński et al. 1995) with 18 reported events and DUO (Alard et al. 1995) with some 10 reported events. New efforts to detect the microlensing of unresolved stars in M31 are being undertaken by the AGAPE (Ansari et al. 1997) and VATT/Columbia (Crotts & Tomaney 1996) collaborations. Reviews of the field of gravitational microlensing are presented in Gould (1996) and Paczyński (1996).

Statistical analysis of an ensemble of microlensing events provides a useful discriminant between Galactic structure models. Two years of observations toward the LMC yield a microlensing optical depth representing approximately 50% of a "standard" Galactic halo comprised entirely of massive compact halo objects (Alcock et al. 1998). Similar analysis of Galactic bulge data, as reported by MACHO and OGLE (Alcock et al. 1997; Udalski et al. 1994a), indicate an optical depth a factor of ~ 3 larger than predicted by axisymmetric Galactic models (e.g., Griest et al. 1991; Paczyński 1991). Consistent Galactic models that include a Galactic bar viewed nearly end-on have recently been constructed (Kiraga & Paczyński 1994; Zhao, Rich, & Spergel 1996; Binney Gehrard, & Spergel 1997). However, it is difficult to identify clearly a lensing population because the mass, velocity, and distance of each lens are not uniquely determined in the standard microlensing solution.

Gravitational microlensing is characterized by the transient, achromatic brightening of a background star due to gravitational deflection of its light by a massive "lens" passing near our line of sight to the source. This results in the distortion of the source disk into multiple (unresolved) images whose total brightness is greater than that of the original source brightness. Given the assumptions of a point-mass lens, point source, and unaccelerated motion, the source magnification $A(t)$ is of the simple form

$$A(t) = \frac{u^2 + 2}{u\sqrt{u^2 + 4}} ,$$

where

$$u(t) = \sqrt{u_{\min}^2 + [2(t - t_0)/\hat{t}]^2} . \tag{1}$$

These equations describe the event's "light curve" as a function of time. $A(t)$ is the observed source magnification, $\hat{t} = 2R_{\mathrm{E}}/v_\perp$ is the characteristic event timescale, where $v_\perp$ is the transverse velocity of the lens, and

$$R_{\mathrm{E}}^2 \equiv \frac{4GM}{c^2} x(1 - x)L \tag{2}$$

is a conveniently defined distance scale in the lens plane (the lens's Einstein radius). M is the mass of the deflector, and x is the ratio of the observer-lens to observer-source (L) distances. The equation for $u(t)$ describes the impact parameter of the lens, scaled by R_{E}, as it passes near the source, and t_0 and $u_{\min}$ are the values of t and u at peak magnification.

Fitting a normal microlensing event provides only one parameter, $\hat{t}$, containing information about the lens. However, $\hat{t}$ is a function of the three unknowns M, x, and $v_\perp$. (Strictly speaking, the source distance L is also unknown, but the uncertainty in L is typically much smaller than that in x, so it is simpler to treat L as known.) This indicates a continuum of event parameters which can conspire to produce similar duration microlensing events.

2. LIGHT-CURVE FINE STRUCTURE AND EXTENDED SOURCE EFFECTS

In instances where the standard approximations break down, light-curve fine structure describes deviations from the standard model whose nature may break this degeneracy. Important microlensing events in this regime include the detection of binary microlensing (Udalski et al. 1994b; Pratt et al. 1996; Alard, Mao, & Guibert 1995; Bennett et al. 1997; Bennett et al. 1996; Alcock et al. 1996d), and the observation of parallax in a gravitational microlensing event (Alcock et al. 1995b). An exciting possibility is the detection of short-timescale deviations in an event light curve due to the presence of planets in the "lensing zone" of the microlensing system (Mao & Paczyński 1991; Gould & Loeb 1992; Bennett & Rhie 1996).

The effects of extended source size may also become apparent in the limit of a large-source, high-magnification event, where the lens impact parameter is of the order of the projected source radius (Goule 1994; Nemiroff & Wickramasinghe 1994; Witt & Mao 1994; Peng 1997). In this situaton, an extra parameter is included in the microlensing solution, $u_* = xR_*/R_{\mathrm{E}}$. Here R_* is the radius of the source star, and u_* describes its projection into the lens plane, scaled by R_{E}. Due to its geometric nature, $u(t)$ is not changed by this parameterization. An analytic solution for $A(t)$ in this limit is presented in Witt & Mao (1994).

Fitting the light curve with the extra parameter u_* provides a second constraint equation for the three lens parameters: the angular size of the source in terms of the lens's Einstein radius. If we estimate the linear radius and distance of the source star from photometry and spectroscopy, we have an estimate of the lens proper motion relative to the source, which leads to a unique mass-distance relation for the lens. Such a situation is rare, and would be expected in only ~ 5% of events toward the Galactic bulge (Gould & Welch 1996).

To account for limb darkening of the source, an appropriate limb-darkening law and coefficients must be determined for the source star. The magnification is then integrated over the face of the star, properly weighted by the brightness profile. The limb-darkening law we will choose is of the form (e.g., Claret, Díaz-Cordovés, & Giménez 1995)

$$\frac{I_\lambda(\mu)}{I_\lambda(1)} = 1 - a(1 - \mu) - b(1 - \mu)^2 . \tag{3}$$

Here μ is the cosine of the angle between the observer's line of sight and the emerging stellar radiation, and a and b are model parameters dependent primarily upon the effective temperature and surface gravity of the star.

TABLE 1

GLOBAL MICROLENSING ALERT NETWORK

Observatory	Latitude, Longitude	Aperture (m)	Detector	Plate Scale (arcsec pixel^{-1})
MSO[a]	149 00.5 E, 35 19.2 S	1.27	8 × 2048 × 2048 Loral	0.63
CTIO[b]	70 48.9 W, 30 30.9 S	0.9	1024 × 1024 Tektronics	0.40
MJUO[c]	170 27.9 E, 43 59.2 S	0.61	1536 × 1024 KAF1600	0.23
UTSO[d]	70 42.0 W, 29 00.5 S	0.61	512 × 512 Photometrics	0.45
WISE[a]	34 45.8 E, 30 35.8 N	1.0	1024 × 1024 Tektronics	0.70

NOTE.—Latitude and longitude are given in degrees and arcminutes.
[a] Mount Stromlo Observatory, Canberra, Australia.
[b] Cerro Tololo Inter-American Observatory, Cerro Tololo, Chile.
[c] Mount John University Observatory, Lake Tekapo, New Zealand.
[d] University of Toronto Southern Observatory, Las Campanas, Chile.
[e] Wise Observatory, Mitzpe Ramon, Israel.

3. GLOBAL MICROLENSING ALERT NETWORK (GMAN)

To provide both the temporal and photometric resolution necessary to distinguish light-curve fine structure, coordinated follow-up observations are being undertaken through the Global Microlensing Alert Network (GMAN) (Pratt et al. 1996; Alcock et al. 1996a), as well as by the PLANET Collaboration (Albrow et al. 1997).

GMAN utilizes telescope resources at Cerro Tololo Inter-American Observatory[31] (CTIO [National Optical Astronomy Observatories]), Mount John University Observatory (MJUO), University of Toronto Southern Observatory (UTSO), and Wise Observatory, which respond nightly to the dynamic status of ongoing microlensing events (see Table 1). Observations from MJUO are carried out by the MOA collaboration of Japan and New Zealand, which is undertaking a general survey of microlensing events toward the Magellanic Clouds and the Galactic bulge (Abe et al. 1997). The observational flexibility available at these locations provided nearly continuous coverage of this event.

Microlensing follow-up images are automatically processed on site. Photometry is carried out using IRAF[32] scripts which call DaophotII (Stetson 1994a). Reductions are usually finished within 6 hr of image acquisition. Team members have immediate network access to GMAN data, which were subsequently used for real-time scheduling during this event. Normalization is performed on the fly using a list of reference stars obtained from the MACHO data set. The reported DaophotII error bars for UTSO and Wise photometry have been increased by a factor of 2.0, to account for the typical scatter in a time series of constant stars from these images. The MJUO data used in this analysis were obtained manually from the raw frames after the event, using DaophotII operating within the IRAF environment; the uncertainties were estimated by examining the variations of standard star ratios within and between frames. Data from CTIO were rereduced using Allframe (Stetson 1994b).

The system and data collection of the MACHO experiment are described in Alcock et al. (1998). The data are obtained simultaneously in two specially designed wide-pass filters with effective wavelengths of approximately 5150 and 6900 Å. Transformations from the MACHO instrumental photometry system to the standard V and R_{KC} (Kron-Cousins) system have been derived by comparisons with several thousand tertiary standard stars calibrated in the LMC. Checks of our photometry with published photometry in Baade's window confirm a zero-point uncertainty of less than 0.1 mag in V and R, where this uncertainty is a conservative estimate of small zero-point differences between fields monitored by MACHO in the bulge.

[31] Operated by the Association of Universities for Research in Astronomy (AURA), Inc., under cooperative agreement with the National Science Foundation.

[32] IRAF is distributed by the National Optical Astronomy Observatories, which is operated by AURA, Inc., under contract to the National Science Foundation.

4. PHOTOMETRY OF MACHO ALERT 95-30

The source star in Alert 95-30 is located at $\alpha = 18^h07^m04^s.26$, $\delta = -27°22'06''$ (J2000). The MACHO project's identifier for this star is 101.21821.128. Alert 95-30 was detected by the MACHO Alert system at $A \sim 1.8$ on 1995 July 24, approximately 22 days before the observed peak.

The location of the source star in an optical color-magnitude diagram (CMD), $V = 16.21$ and $(V-R) = 1.39$, indicates this star passes the "clump giant" cuts defined in Alcock et al. (1997b). Figure 1 shows a single-epoch CMD for a $2' \times 2'$ field surrounding the source star, which is indicated with a circle. We may be reasonably sure, then, that this star is located in the Galactic bulge and has a large radius. Microlensing fits to the rising portion of the light curve predicted a high-magnification event for the giant source, which presented the possibility of source star resolution.

Subsequent observations indicated deviations from the standard microlensing model at $A \sim 20$, approximately 2 days before the projected peak. At this time, we mounted an aggressive program of photometry and spectroscopy to study these deviations thoroughly. Follow-up observations continued nightly past the observed peak until the star returned to its baseline state. Intermittent observations followed to determine accurately the baseline flux as measured at each site.

Figure 2 displays the MACHO 1995 bulge season light curve of Alert 95–30[33]. The alert date is indicated with an arrow, after which time the light curve becomes heavily sampled with follow-up data. Data from all follow-up observatories have been included after determining the

[33] We report an uncataloged CCD trap that allowed several contaminated MACHO red observations to pass through our processing stream. The majority of these were removed from the data set based upon their proximity to the bad columns and point-spread function (psf) FWHM.

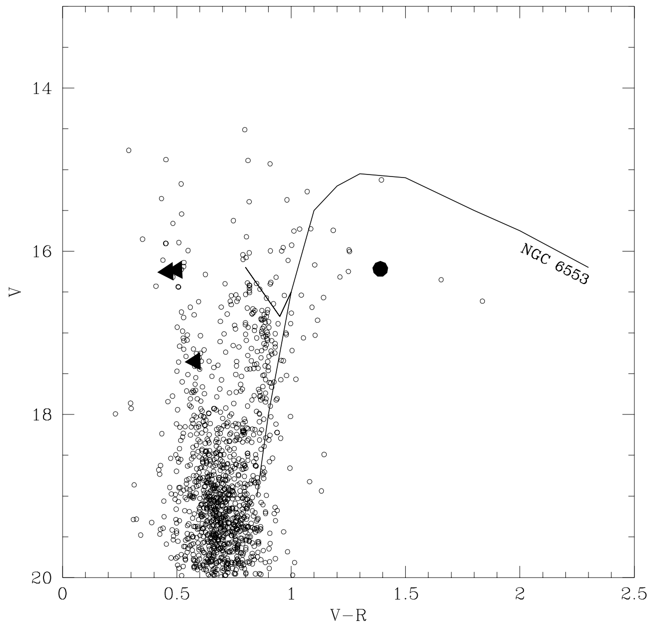

FIG. 1.—Single-epoch V vs. $V-R$ color-magnitude diagram of the field surrounding the source star (*filled circle*). Three RR Lyr (*triangles*) used to estimate the reddening are plotted. The fiducial loci of the giant branch of the metal-rich globular cluster NGC 6553 ([Fe/H] $= -0.2$) from Ortolani et al. (1990) is also indicated.

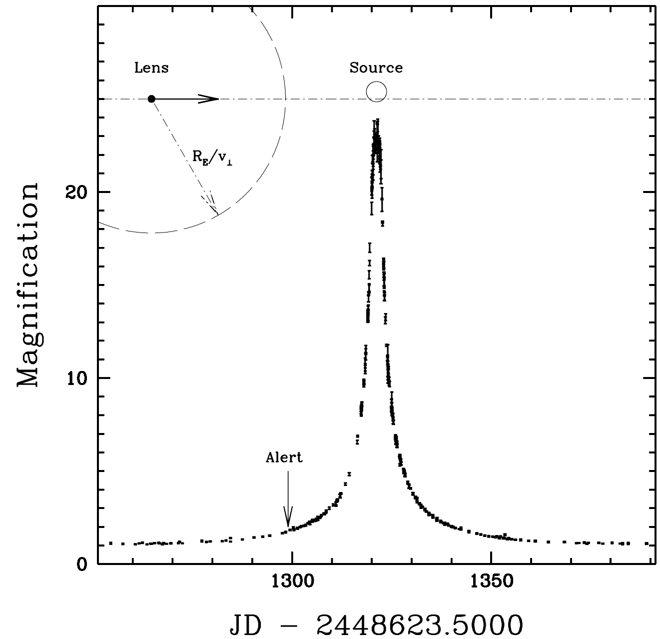

FIG. 2.—1995 light curve of MACHO Object 101.21821.128 (Alert 95-30). The data represent MACHO-GMAN observations of this event in all passbands within a window of 70 days around peak magnification. The date this event was detected by the MACHO Alert system is indicated with an arrow. An additional schematic relates the scale of the lens's Einstein radius to the angular size of the source star, and indicates transit of the lens across the source face.

baseline flux in each passband. No microlensing fits are included in the figure, but it is apparent that the data conform to the symmetric and achromatic shape expected of gravitational microlensing events, at least for magnificaton $A \leq 20$.

This conclusion is confirmed after fitting a normal microlensing curve to the combined data set. Event parameters for this fit (hereafter fit 1) are listed in Table 2, and χ^2 statistics for each passband are listed in Table 3. However, near the peak of the event the data deviate from the expected light curve (see Fig. 3). This type of deviation is not unexpected in a high-magnification microlensing event. We note that the standard point-source microlensing model allows infinite magnification when the source and lens are aligned. When the extended size of the source is considered, the magnification is limited, as the entirety of the source disk cannot be perfectly aligned with the lens. If we include an extra parameter in the fit to account for the angular size of a constant surface brightness source star (fit 2), we reduce χ^2 by 1084. The deviations near the peak of MACHO 95-30 are significantly reduced with this model, which we interpret as clear justification for the extended source microlensing interpretation.

The data in Table 3 indicate an extended source fit χ^2 per degree of freedom of approximately 1 for the GMAN follow-up data. The implication here is that the data scatter around the fit is what one would statistically expect due to measurement error. Thus, the data are in excellent agreement with the extended source microlensing fit, considering our photometry is at the 1%–2% level, as indicated in column (3) of Table 3. However, the MACHO data exhibit $\chi^2_{\rm dof}$ between 3 and 4, which formally indicates a poor fit to the data. While it is obvious that this is indeed a gravita-

TABLE 2

MACHO ALERT 95-30 MICROLENSING STATISTICS

Fit[a]	t_0 [b]	$\hat{t}$ [c]	$u_{\rm min}$	u_*	ω [d]
1......	1321.2 (1)	67.70 (13)	0.04069 (12)	0	?
2......	1321.2 (1)	67.36 (1)	0.05579 (1)	0.07335 (1)	22.1 (30)
3......	1321.2 (1)	67.28 (27)	0.05408 (20)	0.07561 (9)	21.5 (29)

NOTE.—A comparison is shown of event parameters between microlensing fits for MACHO Alert 95-30. Statistics are derived from simultaneous fits on all passbands. Reported uncertainties in the final significant digit(s) are the maximum extent of the surface in parameter space which has a χ^2 greater than the best-fit value by 1.

[a] Fit 1 is the best standard microlensing fit to the data, fit 2 incorporates the extended size of the source star, and fit 3 takes into account limb darkening of the source.

[b] JD $-2{,}448{,}623.50$.

[c] Einstein diameter crossing time.

[d] Lens angular velocity, relative to the source, is in km s^{-1} kpc^{-1} and assumes a $61 \pm 12\ R_\odot$ source at 9 kpc.

TABLE 3

MACHO ALERT 95-30 MICROLENSING STATISTICS

Passband (1)	Number of Observations (2)	$\overline{dm}$[a] (3)	Fit 1 χ^2 (4)	Fit 2 χ^2 (5)	Fit 3 χ^2 (6)
MACHO R	205	0.018	980.33	847.49	839.15
MACHO V	292	0.023	1069.65	964.16	963.86
CTIO R	103	0.019	307.58	124.97	126.51
MJUO R	41	0.019	184.56	46.68	42.62
UTSO V	55	0.020	101.34	48.64	50.28
UTSO R	96	0.013	488.20	82.91	90.09
WISE R	12	0.013	80.71	13.76	7.22
Total	804	...	3212.40	2128.64	2119.76

NOTE.—Individual microlensing statistics are given for MACHO and GMAN observations of Alert 95-30. The numbers of constraints per passband for fits 1, 2, and 3 are 4, 5, and 5, respectively.

[a] Average error, in magnitudes for each passband.

tional microlensing event, such a poor fit might cast doubt on the extended source interpretation. Fits to data of magnification $A < 10$, which should be negligibly affected by extended source effects, display the same excessive scatter around the fit. We conclude that the majority of this scatter is contained in baseline measurements, and should not adversely affect our interpretation of the data.

Figure 2 also presents a scaled schematic of this microlensing event using event parameters derived from fits with a limb-darkened source star (Table 2, fit 3). Included are the lens's Einstein radius expressed as $\hat{t}/2$, and the source radius scaled to $0.0756 R_E$. The trajectory of the lens across the extended face of the source star is shown with $u_{min}/u_* = 0.715$.

Figure 3 provides a visual comparison between the best standard microlensing fit to the data (*dashed line*) and microlensing of a limb-darkened extended source (*solid line*). Each passband was fitted independently with a baseline parameter, while event parameters were derived from joint fits on the combined data set. All fits were performed in the MINUIT environment (James 1994).

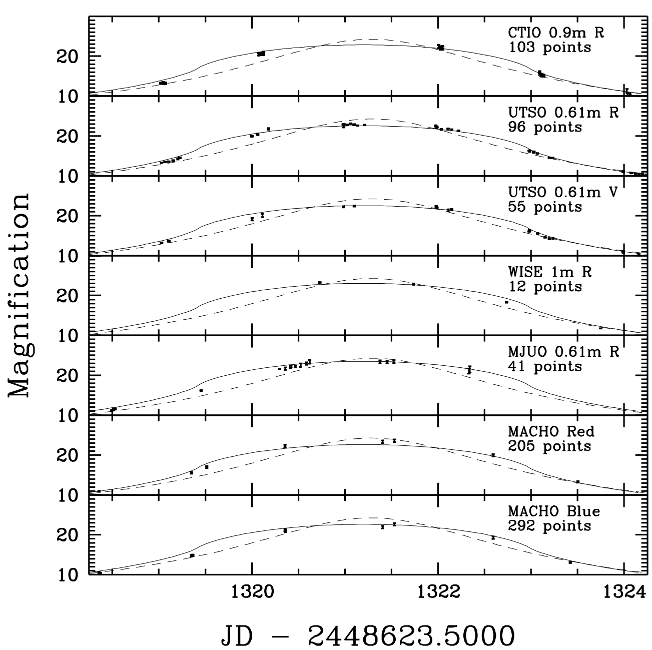

FIG. 3.—Peak of MACHO Alert 95-30, showing the best standard microlensing fit to the data (*dashed line*) and an extended source microlensing fit incorporating source limb darkening (*solid line*).

5. DETERMINATION OF STELLAR PARAMETERS

Analysis of the stellar parameters of the source star in MACHO 95-30 (hereafter referred to as the source star) is required if we are to use the additional information provided by u_* to characterize the lensing object. The most important parameters are its distance (L) and radius (R_*). Also valuable are estimates of the source temperature and surface gravity, which will help define the limb-darkening coefficients.

Figure 1 shows the fiducial line for the red giant branch of the metal-rich globular cluster NGC 6553 from Ortolani, Barbuy, & Bica (1990), plotted over the optical CMD for a $2' \times 2'$ field surrounding the source star. We note that the horizontal branch (HB) in this field is inclined in the same way as that of NGC 6553, due to the effect of differential reddening. Even though the morphology of the red giant branch of this cluster is similar to that of the MACHO field surrounding the microlensing event, the magnitude of the source star is fainter than expected, after we account for the different reddenings and distances to these sources (we adopt a bulge distance of 8 kpc). The smaller apparent luminosity could be due to differences in age, metallicity, or distance. From this diagram, we tentatively conclude that this star is either more metal-rich or more distant (or both) than the giants of similar color in NGC 6553, which are 8 kpc distant.

5.1. *Reddening*

The reddening is patchy in the MACHO field where the source star is located. Figure 4 shows the amplitude versus color of all the RR Lyrae stars that we found in this field. The reddening vector is horizontal in this figure, so the color spread is mostly caused by differential reddening within the field, as the RR*ab* sequence in such a diagram should be very tight (Bono et al. 1997). There appear to be two zones of different obscuration, with $E(B-V)$ ranging from 0.3 to 0.8 mag. The source star appears to be located in the region with smaller reddening, as measured from the colors of the three closest RR Lyrae stars. We identified a total of two bulge RR Lyrae type *ab*, and one RR Lyrae type *c*, within $2'$ of the source star. The locations of these

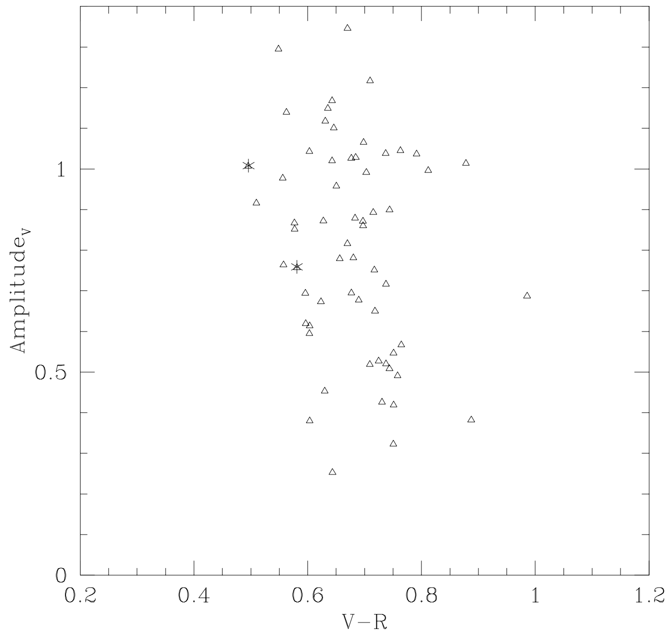

FIG. 4.—Amplitude vs. color of the RR Lyrae type *ab* in the MACHO field where the event is located. The two RR*ab* stars closest to the source star are indicated (*asterisks*). We find $A_V = 1.35$ mag.

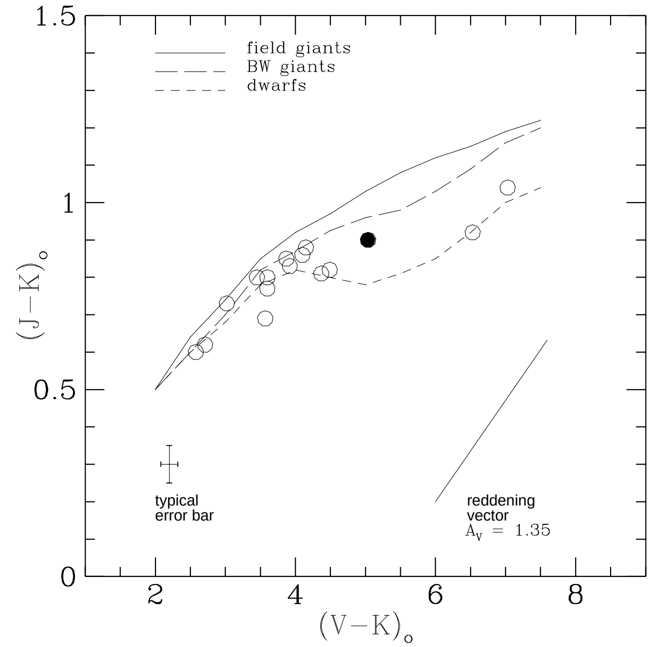

FIG. 5.—Optical-infrared $(V-K)_0$ vs. $(J-K)_0$ color-color diagram for the giants brighter than 1 mag above the horizontal branch in the field surrounding the source star. The fiducial loci of field giants, dwarfs, and Baade's window giants from Frogel & Whitford (1987) are indicated (*solid, short-dashed, and long-dashed lines, respectively*).

three RR Lyrae stars are shown in the optical CMD (Fig. 1, *triangles*). The mean color of the two RR*ab*'s is $V-R = 0.54$, and the mean color of the RR*c* is $V-R = 0.46$. From these colors we deduce $E(V-R) = 0.34 \pm 0.05$. Using the extinction law of Rieke & Lebofski (1985), we obtain $A_V = 1.36$, $E(B-V) = 0.44$, $A_K = 0.15$, $E(V-K) = 1.21$, $E(J-H) = 0.15$, $E(H-K) = 0.08$, and $E(J-K) = 0.23$. The observed and dereddened photometric measurements of the source star are listed in Table 4.

5.2. *Infrared Photometry*

We observed the field of the source star with the CIRIM camera on the CTIO 1.5 m telescope. The f/13.5 configuration yields a pixel scale of 0″.65 pixel^{-1}. The detector is a 256 × 256 HgCdTe NICMOS3 array. Conditions on the night of 1996 September 24 were photometric. We used the J, H, and K_s filters, and a five-position on-source dithering pattern optimally to expose the target field and collect the necessary frames for sky flats. Six, 10 s co-adds were obtained at each position in the dithering pattern for total exposures of 300 s in each filter. The individual IR images were reduced following standard procedure using dark and sky frames, then shifted and combined to create the final images, which cover about 2′ on a side. The photometric calibration was obtained by observing the UKIRT Faint Standard Star 1 (G158-100) just prior to observing the field of the source star. The standard star and program field were observed at identical air masses ($X = 1.2$); thus no extinction corrections were necessary. We find $K = 9.98$, $(J-K) = 1.12$, and $(H-K) = 0.26$ mag for the source star. We estimate an uncertainty of 0.05 mag in J, H, and K from the photon statistics and aperture corrections. Figure 5 shows the optical-IR color-color diagram of stars 1 mag brighter than the horizontal branch in the 2′ × 2′ field surrounding the source star, along with the sequences corresponding to field giants, field dwarfs, and Baade's window giants from Frogel & Whitford (1987). The colors of the source star are similar to Baade's window M giants, and we conclude that it is unlikely to be a field dwarf.

Figure 6 shows an expanded version of the reddening-corrected K_0 versus $(V-K)_0$ optical-IR CMD for the bright stars found in this field. Overplotted are the fiducial lines corresponding to the red giant branches of the metal-rich-globular cluster 47 Tuc from Frogel, Persson, & Cohen (1981) and the metal-rich globular cluster NGC 6553 from Guarnieri et al. (1996), assuming a distance of 8 kpc for both

TABLE 4

PHOTOMETRY OF THE SOURCE STAR IN MACHO 95-30

			ABSOLUTE MAGNITUDE	
Observed	Extinction	Dereddened	8 kpc	9 kpc
$V = 16.21$	$A_V = 1.35$	$V_0 = 14.86$	$M_V = +0.34$	$M_V = +0.09$
$K = 9.98$	$A_K = 0.15$	$K_0 = 9.83$	$M_K = -4.69$	$M_K = -4.94$
$V-R = 1.39$	$E(V-R) = 0.34$	$(V-R)_0 = 1.05$	...	...
$J-K = 1.12$	$E(J-K) = 0.23$	$(J-K)_0 = 0.89$	...	...
$H-K = 0.26$......	$E(H-K) = 0.08$	$(H-K)_0 = 0.18$	...	...
$V-K = 6.23$	$E(V-K) = 1.21$	$(V-K)_0 = 5.03$	...	...
Bolometric		$BC_K = -2.7 \pm 0.1$	$M_{bol} = -2.0$	$M_{bol} = -2.25$

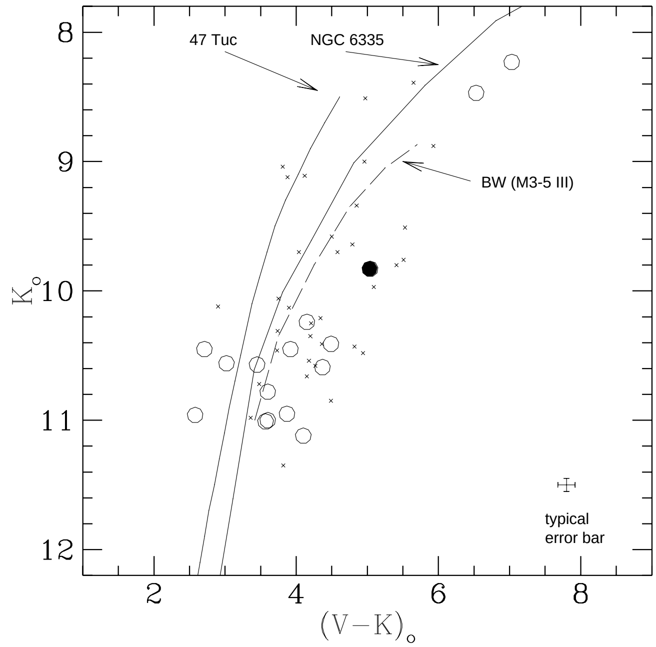

FIG. 6.—Optical-IR K_0 vs. $(V-K)_0$ color-magnitude diagram of the field surrounding the source star. The fiducial loci of the giant branches of the metal-rich globular clusters 47 Tuc ([Fe/H] = −0.7), and NGC 6553 ([Fe/H] = −0.2) from Guarnieri et al. (1996) are indicated. Additionally, we have plotted BW M3–M5 giants (Frogel & Whitford, 1987) (*small crosses*) and drawn our own estimated fiducial line through these points.

populations. Figure 6 shows again that the source star is relatively faint with respect to the giants in these clusters. This suggests that the star is more metal-rich than [Fe/H] = −0.4, and/or more distant than 8 kpc. As an additional comparison, we have plotted data from Frogel & Whitford (1987) for spectral type M3–M5 giants from Baade's window (BW) (assuming a distance of 8 kpc), and our own estimated fiducial line for these stars. If we assume a solar composition for the source star ([Fe/H] = 0), we obtain a distance of about 10 kpc. The uncertainty in this distance is large; it assumes that all of the scatter about the fiducial line of BW giants is due to the line-of-sight depth of the bulge. It is possible that the source star is on the metal-rich tail of the distribution of bulge giant metallicities. Comparing the two globular cluster tracks in Figure 6 gives one a sense of the dependence of the red giant branch fiducial lines on metallicity. If the location of the source star in the CMD were entirely due to metallicity, it would be an extremely metal-rich star, which is less probable than a combination of distance and metallicity effects at work. Given the position of the source star in the CMD at the outer envelope of giants observed in Baade's window, we conclude that the source star is likely located on the "far" side of the bulge. Note that we would expect a giant star in the Sagittarius dwarf galaxy to be about 2 mag fainter than the observed K_0 magnitude of the source star (see also § 5.3.3 below).

5.3. *Spectroscopy*

We have obtained spectra of the source star in several different observing runs, as will be discussed in § 7. Here we analyze the spectra taken at the 4 m Blanco telescope at CTIO with the Ritchey-Chrétien spectrograph and the Loral $3K_1$ detector during the nights of 1995 August 14 and 15, and 1995 September 27. The first two spectra were taken 0.5 days before and after, respectively, the peak of the microlensing event, while the lens was still in transit across the source face. The wavelength coverage of these spectra is from 6230 to 9340 Å. A HeNeAr comparison lamp was used, which provided the wavelength calibration. The exposures were 60 s long, and were taken at an air mass of 1.7. All the spectra were reduced in the standard way. The dispersion was 1 Å pixel^{-1}, and the resolution was 5 Å, as measured from the FWHM of the lines.

The additional spectrum from 1995 September 27 was taken at an airmass of 1.1, with a total exposure time of 500 s. No independent wavelength calibration was obtained for this spectrum. The dispersion was 2 Å pixel^{-1}, and the resolution was 8 Å. The wavelength coverage of this spectrum, shown in Figure 7, was from 3890 to 9830 Å. This spectrum, taken 42.3 days after peak magnification, is very similar to the near-peak spectra. This further supports the microlensing interpretation, where the overall colors or spectral type must not change.

5.3.1. *Spectral Typing*

We determined the spectral type of the source star by direct comparison with the digital spectral atlas of the late-type stars of Turnshek et al. (1985) and Kirkpatrick, Henry, & McCarthy (1991). This comparison was done visually after rebinning our CTIO spectra to lower resolution, and paying close attention to the match of the prominent TiO bands. There is a very close match of the spectra shown in Figure 7 with a spectral type M4 III, and we adopt this classification for the source star. The uncertainty in this classification is estimated to be one spectral subtype.

Using the spectral type, we can check our estimate of the reddening of the source star by adopting the unreddened optical and infrared colors of the same type bulge giants. For an M4 III bulge star, Frogel & Whitford (1987) give $(J-K)_0 = 0.90$ and $(H-K)_0 = 0.18$, and from the observed infrared colors we compute $E(J-K) = 0.22$, and $E(H-K) = 0.08$, respectively. These reddening values are in excellent agreement with the reddening derived from the optical photometry of the RR Lyrae stars in this field (see Table 4).

5.3.2. Ca II *Triplet*

The CTIO spectra allow us to determine independently the surface gravity (g) of the source star. The spectral region

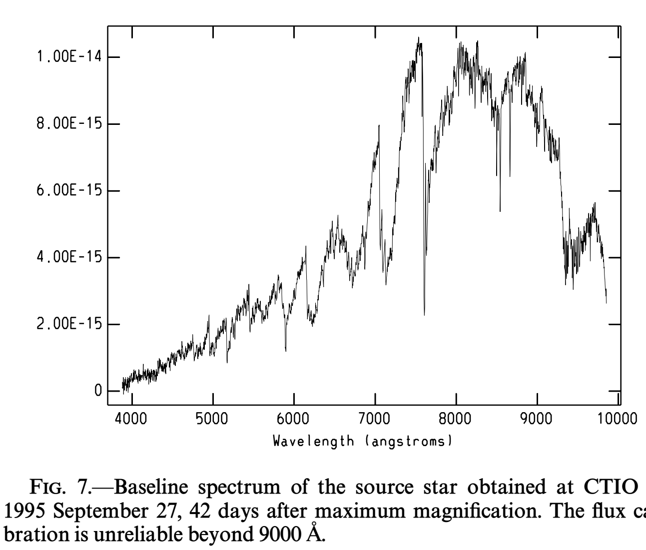

FIG. 7.—Baseline spectrum of the source star obtained at CTIO on 1995 September 27, 42 days after maximum magnification. The flux calibration is unreliable beyond 9000 Å.

covered includes the Ca II triplet, which is strong and very sensitive to log g. Other spectral lines in the region from 6400 to 9200 Å can be used for this purpose in M-type stars, like the Na I doublet at 8183, 8195 Å (Kirkpatrick et al. 1991). However, the lines of the Ca II triplet are the most suitable ones, because they have been studied and calibrated by a number of authors (Jones, Alloin, & Jones 1984; Humphreys & Graham 1986; Diaz, Terlevich, & Terlevich 1989; Alloin & Bica 1989; Jorgensen, Carlsson & Johnson 1992; Erdelyi-Mendez & Barbuy 1991).

We measured the equivalent width (EW) of the Ca II lines at 8498.06, 8542.14, and 8662.17 Å in the three spectra obtained with two different resolutions, obtaining EW $= 11.0 \pm 0.5$ Å, where the uncertainty is dominated by the location of the continuum. We used the local continuum bands at 8480, 8635, and 8905 Å, defined by Jones et al. (1984), Diaz et al. (1989), and Alloin & Bica (1989), in order to make a direct comparison with their measurements and models. Note that the resolution of our spectra is similar to those in the previous works.

We have also compiled published data (spectral type, $T_{\rm eff}$, log g, and Ca II EW) on M-type stars, covering a wide range of temperatures and gravities. In some cases only the two strongest lines of the Ca II triplet are measured, and we have scaled these accordingly in order to include the weaker line, Figure 8 shows the equivalent width versus M spectral subtype for dwarfs (V), giants (III), and supergiants (I). The position of the source star is shown with the box. This figure confirms the conclusions drawn from the IR photometry and spectral classification: the source is a giant star.

Figure 9 shows equivalent width versus log g. The dotted lines show the $\pm 1\ \sigma$ measurements for the source star. From this figure we conclude that log $g = 1.0 \pm 0.2$. A similar value is obtained by applying the empirical relations found by Alloin & Bica (1989) and Diaz et al. (1989), and by slightly extrapolating the models of Jorgensen et al. (1992) and Erdelyi-Mendez & Barbuy (1991).

Diaz et al. (1989) conclude that there is an almost one-to-one correlation between the Ca II triplet EW and surface gravity for stars with solar and higher metallicity. Note that we have assumed solar abundances for the source star. The strength of the Ca II triplet is expected to increase with increasing metallicity, and thus if [Fe/H] > 0, then log $g > 1.0$. We caution that the behavior of this spectral feature as a function of metallicity has not been thoroughly investigated for M-type stars, and we will ignore here this potential source of uncertainty. It does not, however, affect our eventual estimate of the lens proper motion.

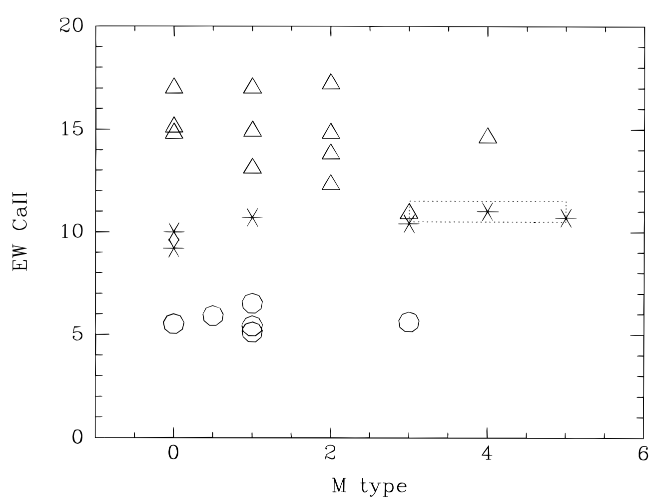

FIG. 8.—Ca II equivalent width in angstroms vs. M spectral subtype for dwarfs (*circles*), giants (*asterisks*), and supergiants (*triangles*). The box encloses the $\pm 1\ \sigma$ measurements of the source star in MACHO 95-30.

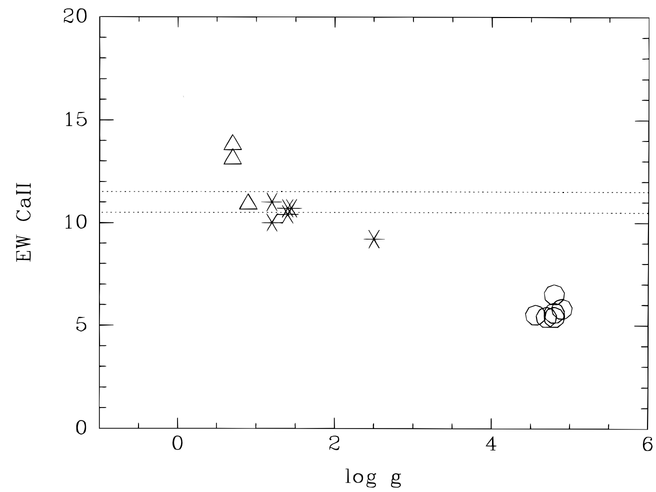

FIG. 9.—Ca II equivalent width (*dotted lines*) of the source star in MACHO 95-30 in angstrom vs. log g ($\pm 1\ \sigma$).

5.3.3. *Radial Velocity*

We have also measured the radial velocity of the source star. Unfortunately, we did not measure radial velocity standards, and have to rely on a wavelength calibration based on the HeNeAr lamps. From the two CTIO spectra of the August run we obtain $V_r = -80 \pm 5$ km s^{-1}. Even though the spectra from the August run have high enough resolution to measure velocities good to less than 10 km s^{-1}, we consider the most important source of uncertainty to be the zero point.

We consider the possibility that the source star may be located in the Sgr dwarf galaxy. The Sgr dwarf galaxy discovered by Ibata, Gilmore & Irwin (1995) is much more extended than previously thought. RR Lyrae stars belonging to this galaxy have been identified in fields close to the Galactic plane (Alard et al. 1996; Alcock et al. 1997). In fact, the Sgr galaxy extends as far as the field containing the source star, as shown by the one Sgr RR Lyrae type *ab* discovered in this field by Alcock et al. (1997). However, the radial velocity measured here rules out membership in the Sgr dwarf galaxy, which has $V_r = +150$ km s^{-1}.

The radial velocities of bulge giants in off-axis bulge fields have been measured by Minniti (1996) and Minniti et al. (1996). At the position of the MACHO field, the mean heliocentric radial velocity of bulge stars is estimated to be about 25 km s^{-1}, with a velocity dispersion $\sigma = 80$ km s^{-1}. The radial velocity of the source star is roughly consistent with the velocities of bulge giants, supporting our assumption that this star belongs to the bulge population.

5.4. *Stellar Parameters*

We will derive the stellar parameters M, $T_{\rm eff}$, L, and R for the source star in a variety of ways and compare the different values to estimate our uncertainties. When needed, we assume the solar values: $T_\odot = 5730$ K, log $g_\odot = 4.44$, and $M_{\rm bol\odot} = 4.72$ mag. The following equations relate various stellar parameters:

$$(L/L_\odot) = (R/R_\odot)^2(T_{\rm eff}/T_\odot)^4$$
$$(g/g_\odot) = (M/M_\odot)(R/R_\odot)^{-2} .$$

We begin with the simplest method, adopting the typical stellar parameters of an M4 giant in the Galactic bulge. We could expect the mass of the source star to be $\sim 1\ M_\odot$, the mass appropriate for a bulge giant according to the estimated age of the bulge (Holtzmann et al. 1993). Using only the spectral type information (M4 III), we obtain $T_{\rm eff} = 3430$, $M_{\rm bol} = -2.7$ from Lang (1922), which gives $R = 85\ R_\odot$. Also, for an M4 III star, $R = 83\ R_\odot$, and $T_{\rm eff} = 3600$ from the recent calibrations of Dyck et al. (1996). These values are averages over several spectral subtypes. The dependence of radius on spectral type is such that for an M3 III star $R \approx 60\ R_\odot$, and for an M5 III star $R \approx 100\ R_\odot$.

The IR colors allow us to measure the effective temperature. For $(J-K)_0 = 0.89$, $T_{\rm eff} = 3900 \pm 270$ from the calibration of Feast (1996). For $(V-K)_0 = 5.03$, $T_{\rm eff} = 3600$ from the recent calibration of Bessell, Castelli, & Plez (1997). The optical photometry also allows us to estimate the temperature of the source star. For $(V-R)_0 = 0.93$, we find $T_{\rm eff} = 3800 \pm 200$ by differential comparison with the giant star III-17 member of the globular cluster NGC 6553 analyzed by Barbuy et al. (1992). Comparing these values of temperature with those derived from the spectral type information, we adopt a temperature of $T_{\rm eff} = 3700 \pm 250$ for the source star, or $\log(T/T_\odot) = -0.19 \pm 0.03$.

Numerous bolometric corrections exist in the literature. We find $BC_K(J-K) = 2.6$ and $BC_K(V-K) = 2.7$ from Frogel & Whitford (1987) and Bessell et al. (1997); BC_H(M giants) = 2.6 from Bessell & Wood (1984); and BC_V(M4 III) = −2.2 (Lang 1992). These give $m_{\rm bol} = 12.4$, 12.5, 12.6, and 12.6, respectively. We adopt $m_{\rm bol} = 12.5 \pm 0.1$ for the source star.

In order to compute the absolute magnitudes, we must assume a distance to the star. Adopting a distance of 8 kpc, or $(m - M)_0 = 14.52$, we obtain the absolute magnitudes $M_V = +0.34$, $M_K = -4.69$, and $M_{\rm bol} = -2.0$ mag. This gives $\log(L/L_\odot) = 2.69 \pm 0.04$. We can immediately derive the radius, $\log(R/R_\odot) = 1.72 \pm 0.06$ or $R = 53 \pm 8\ R_\odot$. However, the uncertainty here is underestimated given the systematic uncertainty in the adopted distance. From our arguments in § 5.2, we adopt the distance to the source star of 9 ± 1 kpc, giving a distance modulus $(m - M)_0 = 14.77 \pm 0.25$. Recalculating the radius at this distance and incorporating the added uncertainty, we find $M_{\rm bol} = -2.25 \pm 0.27$ and thus $R = 61 \pm 12\ R_\odot$.

Last, we derive the mass of the source star using the measured value of $\log g$ (§ 5.3). We find $\log(g/g_\odot) = -3.44 \pm 0.08$ and $M \sim 0.8 - 2.5\ M_\odot$. The mass derived in this manner is quite uncertain. The largest mass values are unlikely given the age of the bulge $t \approx 10$ Gyr (Holtzman et al. 1993). However, a mass slightly larger than $1\ M_\odot$ is consistent with the source star having a high metallicity.

To summarize, we adopt the following stellar parameters for the source star in MACHO Alert 95-30, which we categorize as an M4 bulge giant:

$$L = 600 \pm 200\ L_\odot\ , \quad T_{\rm eff} = 3700 \pm 250\ K\ ,$$
$$\log g = 1.0 \pm 0.2\ , \quad R = 61 \pm 12\ R_\odot\ ,$$
$$D = 9 \pm 1\ {\rm kpc}\ , \quad M \approx 1.0\ M_\odot\ , \quad [{\rm Fe/H}] \approx 0\ .$$

6. DETERMINATION OF EVENT PARAMETERS

6.1. *Effect of Limb Darkening on the Photometry*

We now integrate an approximate limb-darkening law into the microlensing model, to extract more realistic event parameters than those derived with a constant surface brightness disk. Limb-darkening coefficients for GMAN's standard R and V passbands exist in the literature for $T_{\rm eff} = 3500$ K, $\log g = 1$ for the quadratic form of equation (3) (Claret et al. 1995; Díaz-Cordovés, Claret, & Giménez 1995). Limb-darkening coefficients were also calculated for MACHO's nonstandard passbands (A. Claret 1996, private communication). These coefficients are listed in Table 5.

Including this brightness profile in the extended source model further improves the fit χ^2 by 9 (see Table 3, fit 3). While this improvement is formally significant, its interpretation here appears unclear. Comparison of fits 2 and 3 in Table 3 shows no clear trend between data sets, which effectively washes out any overall conclusions about the significance of the model. However, we do regard the limb-darkened parameters as the more realistic interpretation of the data. Comparison of optical and infrared photometry during a lens transit should detect significant color terms as a result of source limb darkening (Gould & Welch 1996), which would then provide a more robust test of stellar atmosphere models.

6.2. *Implications for Lens Mass*

The limb-darkened fit to finite source microlensing provides a direct measurement of $u_* \equiv \theta_*/\theta_{\rm E} = 0.0756$, i.e., the angular size of the star as a fraction of the Einstein ring angle. To convert this into physical units, we need an estimate of the angular radius θ_* of the source star. The analysis in § 5 indicates $R_* = 61\ R_\odot$ and $L = 9$ kpc, giving $\theta_* = 31.5\ \mu$as and thus $\theta_{\rm E} = 0.417$ mas. The Einstein diameter crossing time $\hat{t}$ is measured similarly to the usual point-source case, so this provides the proper motion of the lens with respect to the source star $\omega \equiv 2\theta_{\rm E}/\hat{t} = 21.5$ km s^{-1} kpc^{-1} = 4.51 mas yr^{-1}.

Simply adding the fractional errors of R_* and L in quadrature leads to a 23% uncertainty in the lens proper motion. However, the uncertainty in L has been included in the uncertainty in R_* (see § 5.4), so this represents an overestimate of the uncertainty in ω. A similar solution for the lens proper motion may be obtained by deriving the angular size of the source star from $T_{\rm eff}$ and $m_{\rm bol}$ (Gray 1992). These parameters are more tightly constrained than R_* and L, and lead to a smaller fractional error in θ_*. The uncertainty in the angular size of the source star, and therefore of the lens proper motion, is approximately twice the uncertainty in $T_{\rm eff}$, or 13.5%.

TABLE 5

Limb-Darkening Coefficients for the Source Star

Pasband	a	b
MACHO V	1.140	−0.284
MACHO R	0.825	−0.051
Standard V	1.072	−0.228
Standard R	0.910	−0.108

Note.—Table lists limb-darkening coefficients for eq. (3) used to approximate the brightness profile of the source star in MACHO Alert 95-30.

Thus, an extended source microlensing event provides us with two constraints $\hat{t}$ and ω on the three unknowns M, x, and $v_\perp$ of the lens. In the following, it is convenient to define $\hat{v} \equiv \omega L = v_\perp x^{-1}$ to be the relative velocity of the lens projected back to the source plane (see Han & Gould 1996); substituting $r_E = \hat{v}x\hat{t}/2$ into equation (2), we obtain a one-to-one relationship between the lens mass and distance,

$$M(x) = \frac{\hat{v}^2\hat{t}^2c^2}{16GL}\frac{x}{1-x} . \qquad (4)$$

(By symmetry, this is the same as eq. (5) of Alcock et al. 1995b exchanging observer and source, i.e., with $\hat{v}$ instead of $\tilde{v}$, and $x \leftrightarrow 1-x$.) For the observed values of $\hat{v} = 193$ km s^{-1}, $\hat{t} = 67.3$ days, we have $M(x) = 0.192\ M_\odot\ x/(1-x)$; thus the lens may be either a low-mass star roughly half way to the source or a more massive star closer to the source. Figure 10 shows $M(x)$ for the event parameters given in Table 3 (fit 3), and the radius and distance of the source star obtained in § 5. For reference, we also include $M(x)$ contours for $R_* = 61 \pm 12\ R_\odot$.

We may obtain additional constraints on x by using a model for the distributions of sources and lenses, since the likelihood of obtaining the observed value of $\hat{v}$ is also a function of x.

For a given lens mass, the rate of microlensing is proportional to

$$d\Gamma \propto \sqrt{x(1-x)}\rho_L(x)v_\perp f_S(\boldsymbol{v}_S)f_L(\boldsymbol{v}_L)\,dx\,d\boldsymbol{v}_S\,d\boldsymbol{v}_L . \qquad (5)$$

where ρ_L is the density of lenses at distance x and $f_L(\boldsymbol{v}_L)$ and $f_S(\boldsymbol{v}_S)$ are the lens and source velocity distribution functions (normalized to unity) in the plane perpendicular to the line of sight. The source and lens velocities $\boldsymbol{v}_S$, $\boldsymbol{v}_L$ are related to $\hat{\boldsymbol{v}}$ by $\boldsymbol{v}_L = (1-x)\boldsymbol{v}_\odot + x(\boldsymbol{v}_S + \hat{\boldsymbol{v}})$, where $\hat{\boldsymbol{v}} = (\hat{v}\cos\phi, \hat{v}\sin\phi)$ and ϕ is the (unknown) direction of the relative proper motion.

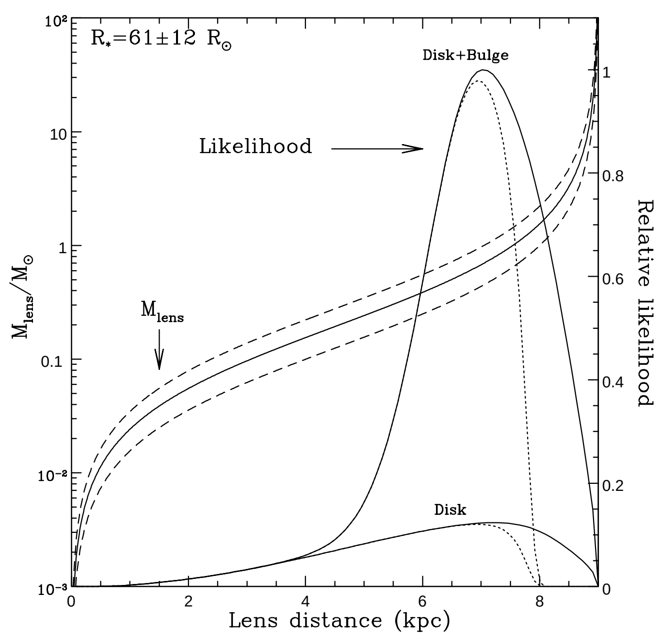

FIG. 10.—Lens mass plotted as a function of its distance, using eq. (4)This assumes a 61 $R_\odot$ source, with error contours provided at $\pm 12\ R_\odot$, and event parameters listed in Table 3 (fit 3). The likelihood curves (*solid lines*) show relative probabilities for disk and bulge lenses as a function of their distance. The dotted lines include an upper limit on the brightness of a main-sequence lens.

Given a model for ρ_L, f_S, and f_L, we may integrate equation (5) and thus obtain joint probability distributions for any of the variables. Since we have measured $\hat{v}$, and the lens mass depends on only one unknown (x), we need to consider the joint probability distribution of events in the (x, $\hat{v}$)-plane, and then marginalize to get a probability distribution of x given the observed value of $\hat{v}$.

Thus, we change variables from $d\boldsymbol{v}_L$ to $d\hat{v}\,d\phi$, giving

$$d\Gamma \propto \sqrt{x(1-x)}\rho_L(x)v_\perp f_S(\boldsymbol{v}_S)f_L(\boldsymbol{v}_L)\,dx\,d\boldsymbol{v}_S \left|\frac{\partial \boldsymbol{v}_L}{\partial(\hat{v}, \phi)}\right| d\hat{v}\,d\phi . \qquad (6)$$

We then substitute, for $\boldsymbol{v}_L$ and $v_\perp$ and integrate over the unknowns $\boldsymbol{v}_S$ and ϕ, giving a likelihood as a function of distance for given $\hat{v}$,

$$\mathscr{L}(x; \hat{v}) = \left.\frac{d\Gamma}{dx\,d\hat{v}}\right|_v \propto \sqrt{x(1-x)}\rho_L(x)\hat{v}^2x^3 \times \iint f_S(\boldsymbol{v}_S)f_L((1-x)\boldsymbol{v}_\odot + x(\boldsymbol{v}_S + \hat{\boldsymbol{v}}))\,d\boldsymbol{v}_S\,d\phi . \qquad (7)$$

This result may be understood as follows: the integrals are over all combinations of source and lens velocity which give rise to the observed $\hat{v}$. The $[x(1-x)]^{1/2}$ and ρ_L terms arise from the x-dependence of the Einstein radius and density of lenses, respectively. There is a factor of $v_\perp = \hat{v}x$ because a given lens contributes a lensing rate $\propto v_\perp$, and a factor of $x^2\hat{v}$ from the Jacobian det $[\partial \boldsymbol{v}_L/\partial(\hat{v}, \phi)]$.

To evaluate equation (7), we adopt a disk velocity dispersion of 30 km s^{-1} in each direction, with a flat rotation curve of 220 km s^{-1}. We adopt a bulge velocity dispersion of 80 km s^{-1} in each direction, and no bulge rotation. For the density profiles, we use a standard double-exponential disk, and a barred bulge as in Han & Gould (1995). The source is located at Galactic coordinates $l = 3\overset{\circ}{.}73$, $b = -3\overset{\circ}{.}30$, and we assume $L = 9$ kpc, $R_0 = 8$ kpc, so the source is behind the Galactic center. We assume the source is a member of the bulge, so we take f_S to be the above velocity distribution function of bulge stars, and then we evaluate equation (7) separately for ρ_L, f_L appropriate for lenses in either the disk or the bulge.

Figure 10 shows the result of equation (7) as a function of lens distance, for the observed $\hat{v} = 193$ km s^{-1}. The lower solid line shows disk lenses only, and the upper solid line shows the sum of disk + bulge lenses; the relative areas indicate that there is about an 80% probability that this lens belongs to the bulge.

We define a median distance $x_{\rm med}$ such that half of the integrated likelihood arises from $x < x_{\rm med}$, giving $x_{\rm med} = 0.77$ and a median mass estimate of $M_{\rm med} = 0.67\ M_\odot$. Similarly, we define a 90% confidence interval (x_1, x_2) such that 5% of the integrated likelihood arises from each of $x < x_1$ and $x > x_2$; the resulting interval is $0.52 < x < 0.943$, which translates into a mass interval of 0.021–3.2 $M_\odot$. These results are relatively insensitive to the details of the galactic model, since the constraints on x are dominated by the drop in $\rho_{\rm bulge}$ for $x \lesssim 0.6$ and by the geometrical factor $[x(1-x)]^{1/2}$ for $x \to 1$.

For reference, Figure 11 shows $\hat{v} \int \mathscr{L}(x; \hat{v})\,dx$, i.e., the lensing rate per unit log $\hat{v}$ for disk and bulges lenses. The observed value of $\hat{v} = 193$ km s^{-1} is well within the range of expected values. The areas under the two curves reflect the fact that bulge lenses produce about three times the event

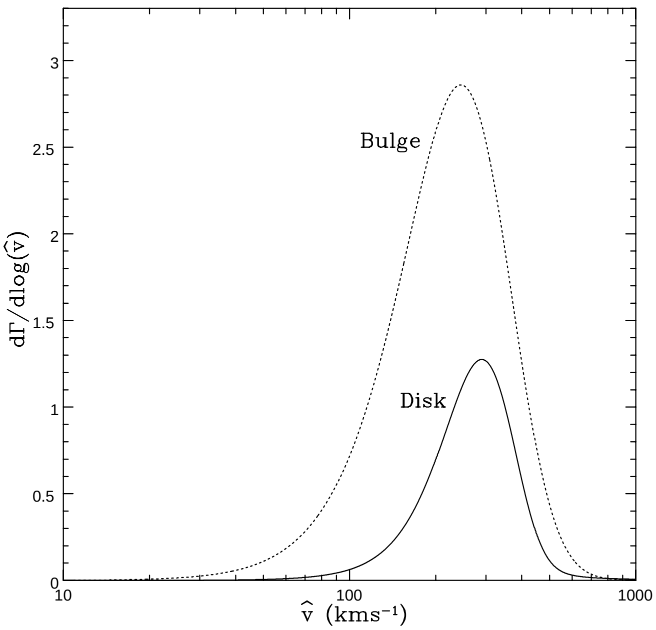

FIG. 11.—Lensing rates per unit log $\hat{v}$ for disk and bulge lenses (*solid and dashed lines, respectively*).

rate of disk lenses for the above models. This figure shows that there is a large overlap in the distributions; events with $\hat{v} \lesssim 150$ km s^{-1} are produced almost entirely by bulge lenses, but the more common events with larger $\hat{v}$ arise from both disk and bulge lenses. Thus, proper-motion measurements toward the bulge are not as useful as parallax measurements for constraining the lens distance. (This has been previously noted by Han & Gould 1995). Note that this is distinctly different from the LMC case, where either proper motion or parallax measurements provide a good separation of the various lensing populations (Gould 1996).

6.3. *Constraints on Lens Luminosity*

As seen above, if the lens is more distant than $x > 0.9$, it has a relatively large mass. If it is a hydrogen-burning star, we can constrain this possibility as follows. For the above proper motion of $\omega \approx 4.5$ mas yr^{-1}, the lens is completely unresolved from the source during our observations; thus the observed light curve of our "object" is simply the sum of light curves from the source, the lens, and possibly other superposed stars.

Any flux from the lens would add a constant unmagnified baseline that would distort the microlensing fit. Although in most cases this additional flux would be a small fraction of the flux of the source star, with the high-precision measurements here this would be detectable even if the lens is considerably fainter than the source.

We have fitted "blended" microlensing to data of magnification $A < 10$. This fit is of the form $f_i(t) = A(t) f_{0i} + f_{Ui}$, where $i =$ each passband, f_{0i} is the baseline flux of the source star, and f_{Ui} is the total flux of unlensed stars superposed on the source, i.e., the sum of flux from the lens and any other superposed stars.

We note that the $\chi^2_{\rm dof}$ values of all light curves in these blended fits are similar to those in the extended source fits. We therefore exclude the MACHO data in our lens brightness estimate because of excessive baseline scatter; however, this turns out to be unimportant. The most follow-up data with $A < 10$ are contained in the CTIO and UTSO observations. For the CTIO R, UTSO R, and UTSO V passbands, we find $f_{Ui}/f_{0i} \approx (-0.021 \pm 0.016)$, (-0.019 ± 0.017), and (-0.015 ± 0.016), respectively, consistent with zero flux from the lens. For completeness, we note that similar results are obtained from the MACHO data, with $f_{Ui}/f_{0i} \approx (-0.012 \pm 0.017)$ and (-0.026 ± 0.018) for MACHO V and MACHO R, respectively. MJUO and Wise data did not contain enough baseline observations to determine accurately the amount of unlensed flux. In the following, we take 0 ± 0.02 as a conservative limit.

If the lens is a main-sequence star, we may predict its apparent brightness using the mass-distance relation of equation (4). Assuming a main-sequence V-band mass-luminosity relation $L/L_\odot = (M/M_\odot)^{3.5}$, and 1.5 mag of extinction, we find that the apparent brightness of a main-sequence lens would be 1% of that of the source star for $x = 0.83$ and 10% for $x = 0.90$. Note that the implied lens brightness *increases* with distance since the rapid rise in $M(x)$ outweighs the r^{-2} term; note also that a giant lens is excluded at any distance.

Instead of applying a sharp limit $x < 0.88$, it is more rigorous to multiply the likelihood function of equation (7) by the Gaussian probability that the lens brightness is consistent with the above constraint on f_U/f_0. This causes a rapid roll-off in the likelihood function for $D_L > 7.5$ kpc, as shown in Figure 10 (*dotted curves*). Assuming a main-sequence lens, we can recompute the constraints on x and M from the likelihood function with the brightness factor, giving a median $x = 0.73$, a mass of $M_{\rm med} = 0.53\ M_\odot$, and 90% confidence intervals of $0.48 < x < 0.84$ and $0.18 < 1.05\ M_\odot$. Thus, the inclusion of the lens brightness constraint reduces the median mass only slightly, but considerably strengthens the upper limit.

7. SPECTRAL VARIATION DURING MACHO 95-30

In addition to the CTIO observations discussed in § 5.3, we have obtained spectra at Mount Stromlo and Keck[34] observatories. Table 6 lists the complete catalog of spectroscopic observations of this event. Figure 12 schematically shows the location of the lens with respect to the source when these different observations were made. Nightly spectra of the source star were taken between 1995 August 18 and 25 (from 2.8 to 9.8 days after peak magnification), with the Cassegrain spectrograph at the Mount Stromlo Observatory (MSO) 74 inch (1.9 m) telescope. They cover the wavelength interval 6240–6770 Å, with a dispersion of 0.90 Å pixel^{-1}, and a resolution FWHM = 4.6 Å as determined from the comparison lamp spectra. The total exposures were typically 1000 s long. These MSO spectra are wavelength-calibrated and sky-subtracted, but not fluxed. The signal-to-noise ratio (S/N) per resolution element is listed in Table 6, along with other relevant data.

The CTIO and MSO spectra have similar resolutions, with the exception of the September 27 CTIO spectrum, which has lower resolution. We rebinned the CTIO and MSO spectra in order to compare them directly. Figure 13 shows the spectral sequence, which constitutes one of the most extensive and homogeneous series of spectroscopic observations of a microlensing event to date (see also

[34] The Keck telescope project was made possible by a generous grant from the W. M. Keck Foundation.

TABLE 6

Summary of Spectral Observations Appearing in Figure 12

JD	Telescope and Spectrograph	Dispersion (Å pixel^{-1})	Resolution (Å)	Coverage (Å)	S/N
2,449,944.234......	CTIO 4m/RC Sp.	1.0	4.0	6230–9340	~100
2,449,945.211......	CTIO 4m/RC Sp.	1.0	4.0	6230–9340	~100
2,449,947.221......	Keck 10 m/HIRES	0.04	0.2	4309–6739	92–256
2,449,947.524......	MSO 74 inch/Cassegrain Sp.	0.9	4.6	6240–6770	106
2,449,948.223......	Keck 10 m/HIRES	0.04	0.2	4835–7282	166–296
2,449,948.504......	MSO 74 inch/Cassegrain Sp.	0.9	4.6	6240–6770	117
2,449,949.509......	MSO 74 inch/Cassegrain Sp.	0.9	4.6	6240–6770	113
2,449,950.322......	Keck 10 m/HIRES	0.04	0.2	3750–6065	20–141
2,449,950.523......	MSO 74 inch/Cassegrain Sp.	0.9	4.6	6240–6770	91
2,449,951.498......	MSO 74 inch/Cassegrain Sp.	0.9	4.6	6240–6770	96
2,449,952.508......	MSO 74 inch/Cassegrain Sp.	0.9	4.6	6240–6770	72
2,449,953.494......	MSO 74 inch/Cassegrain Sp.	0.9	4.6	6240–6770	78
2,449,954.513......	MSO 74 inch/Cassegrain Sp.	0.9	4.6	6240–6770	66
2,449,987.000......	CTIO 4 m/RC Sp.	2.0	8.0	3890–9830	~100

Benetti, Pasquini, & West 1995 and Lennon et al. 1996). It is clear that the microlensing does not change the spectral type of the star, nor does it strongly affect the major spectral features. However, subtle effects may appear in some spectral lines, as discussed by Valls-Gabaud (1994) and Loeb & Sasselov (1995), which warrants a more careful comparison among the spectra.

Before this discussion, we note that the MSO spectrum of August 18 (the first MSO spectra taken *after* the lens transit) is anomalous, showing a dip at 6520 Å that looks like an unidentified band head. Although we have examined several possible sources for this feature, including checking the flat fields and comparing the spectra of other stars in the field, the cause of this dip is still unexplained.

Each spectrum was divided by the median combination of all spectra (this operation was repeated before and after continuum subtraction, in order to account for possible differences due to flux calibration of the CTIO spectra but not of the MSO spectra). Figure 14 shows the sequence of these ratios. While there are no strong deviations, the two spectra taken closest to maximum magnification show stronger Hα than the rest. Also, these two spectra show stronger TiO bands than the following ones. The total TiO absorption, however, started to climb steadily after 1995 August 18. We measured the equivalent widths of several spectral features of interest within 6240–6770 Å with the SPLOT package within IRAF. Figure 15 shows the equivalent width of Hα, and the combined intensity of four TiO bands in the 6650–6750 Å region. Included are conservative error bars based upon uncertainty in placing the local continuum. The equivalent width of the Hα line was scaled to the equivalent width measured in the HIRES spectra of 1995 August 18 and 19. These equivalent widths were measured with respect to the local pseudocontinuum, in the same way as for all the spectra, in order to avoid systematic effects.

While we cannot explain in detail the behavior of these spectral features, changes in the equivalent width of these lines have been predicted by Loeb & Sasselov (1995). These changes caused by limb-brightening effects in the cores of resonance lines (like Hα), a result of a very extended photosphere. Resonant line scattering may also affect the optical TiO bands in the case of M giants like the MACHO 95-30 source (Sasselov 1997). Detailed modeling of the spectra of

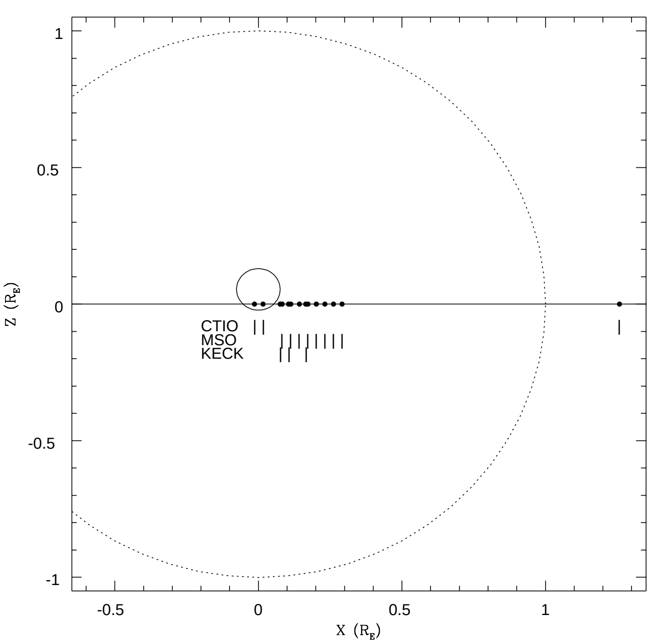

Fig. 12.—Spectral observations listed in Table 6 plotted on the source plane. The relative sizes of the star (*solid circle*) and the lens's Einstein radius (*dotted circle*) are plotted to scale, in units of R_E. The solid points show the position of the lens at the different times when spectra were taken. The observatories where the spectra were taken are indicated by the tick marks.

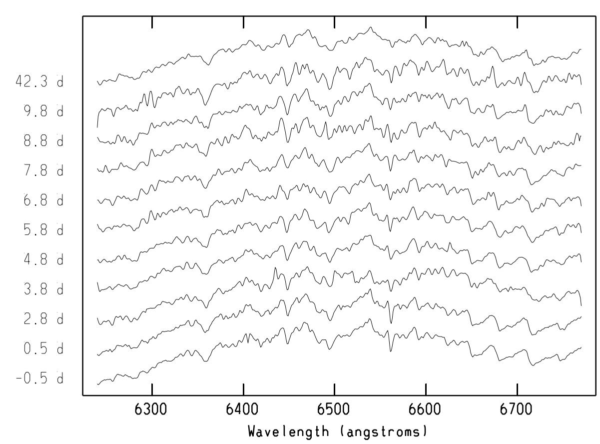

Fig. 13.—Spectra of the source star taken at CTIO and MSO. All of these have similar resolution, except for the top one. Note Hα at 6553 Å, and the TiO band heads at 6647, 6676, 6711, and 6742 Å. Days from the peak of the microlensing event are indicated along the vertical axis.

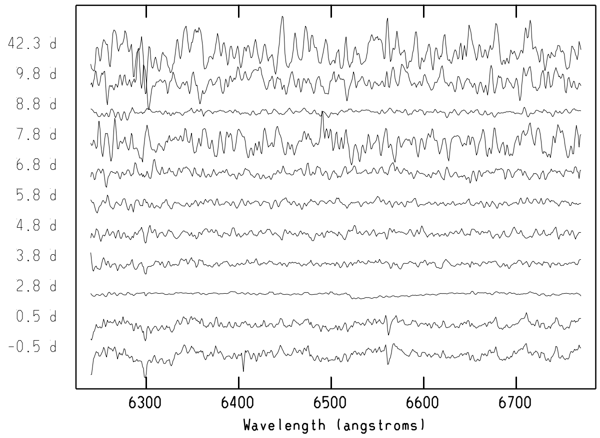

FIG. 14.—Same as Figure 13, showing the spectra divided by the median combination of all. These have been displaced in the vertical direction and arbitrarily scaled, such that the flattest spectra here actually display the largest range of excess from the median combination. Note the changes in Hα and the TiO bands in the two spectra nearest peak magnification.

this event in particular is needed, as it will help with the interpretation of forthcoming similar events.

Three spectra were also taken in the nights of August 18, 19, and 21, about 5 hours earlier than the MSO spectra, using HIRES at the Keck 10 m telescope. These high-resolution spectra also have a high S/N, as listed in Table 6, which includes the S/N per resolution element of the lowest and highest orders. The spectra of August 18, 19, and 21 consist of 30, 25, and 40 orders, respectively. The blue region below about 4000 Å covered in the August 21 spectrum does not have much information due to low counts. We have checked different resonance lines (Ca II, Hα, Hβ, Hγ, etc.) and have found no large variations. The August 21 spectrum has coverage extending to the blue, including the Ca II H and K lines, but misses the Hα line. The spectra of August 18 and 19 do not include these Ca lines. The Hα equivalent width differs by only 4% between August 18 and 19, as measured from the high quality HIRES spectra (1.087 vs. 1.039 Å). This variation occurs in the core of the line. Otherwise, there is no significant change between the Hα profiles of August 18 and 19. The strong TiO band heads at 4954, 5166, and 5447 Å are present in all three HIRES spectra. The difference of about 10% in strength of these bands between August 18 and 21 seen in the MSO spectra is confirmed.

We have also fit the Na I (D) line profiles in the HIRES spectra with an interstellar cloud model which uses 12 clouds over the velocity range from -60.8 km s^{-1} to $+202.3$ km s^{-1}. The clouds with extreme velocities only fit one line of the Na doublet because of problems with the continuum determination and blending with other lines. The interstellar clouds indicate that the star is at a great distance and therefore is certainly a giant, as discussed in § 5.3.

We also measured the radial velocities of the MSO spectra using the cross-correlation routine FXCOR within IRAF. From the MSO spectra, we measure a mean velocity of $V_r = -76 \pm 4$ km s^{-1}, which is in excellent agreement with the mean velocity of $V_r = -80 \pm 5$ km s^{-1} from the CTIO spectra, reduced and calibrated independently (§ 5.3). The velocities of the eight MSO spectra agree with each other within an rms of 12 km s^{-1}. We also measured the radial velocity of the August 21 HIRES spectrum, $V_r = -86.2 \pm 3.9$ km s^{-1}, using the strong Cr lines at 4254, 4274, and 4289 Å. All these velocities are in excellent agreement, and we adopt a final value of $V_r = -81 \pm 5$ km s^{-1} for the source star in MACHO 95-30.

Subtle radial velocity variations (of the order of 1–2 km s^{-1}) may also be expected during microlensing events such as this one (Maoz & Gould 1994), and can give an independent measurement of the proper motion. Alternatively, combining the radial velocity variation with the extended source-magnification effect, one can determine the projected rotation velocity of the star (Gould 1997). We note that detecting such velocity differences may be possible using the HIRES spectra, after detailed corrections and modeling that are beyond the scope of the present paper.

In summary, we have obtained a large number of spectra of the microlensed source star during MACHO Alert 95-30. These spectra show subtle variations, which support the predictions of existing microlensing and stellar models. These spectra demonstrate that differential magnification of an extended source star during a gravitational microlensing event may be used to probe otherwise inacessible stellar atmosphere fine structure.

8. CONCLUSIONS

We have observed the breakdown of the point-source approximation for the first time in a "normal," single-lens microlensing event. This deviation was anticipated based upon real-time information provided by MACHO-GMAN, and dynamically scheduled for GMAN follow-up observations throughout the event. In effect, we have resolved a

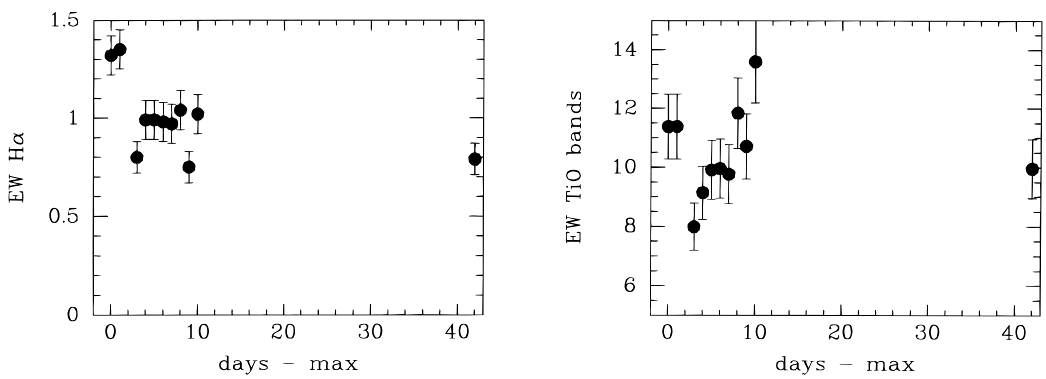

FIG. 15.—Temporal evolution of the equivalent width in angstroms of Hα and the TiO band heads, measured with respect to the local pseudocontinuum. The equivalent widths plotted in the right-hand panel are the sums of the TiO bands at 6647, 6676, 6711, and 6742 Å.

star which is ∼9 kpc from Earth. The resulting deviation from point-source microlensing provides a second constraint equation for the system, partially reducing the ambiguity between lens mass, position, and transverse velocity.

Measurement of the effective radius of the source star during the microlensing event provides an estimate of the scale of the lens's Einstein radius. With additional information about the radius and distance of the source, we determine the angular velocity of the lens with respect to our line of sight to the source. This allows a statistical estimate of the lens mass by assuming velocity distributions of sources and lenses. We conclude that this event is a result of lensing by an object of mass $0.67^{+2.53}_{-0.46}\ M_{\odot}$ (at the 90% confidence level), such as a white dwarf or a neutron star, which is most likely in the bulge (80%). If the lens is a main-sequence star, the upper end of this mass range is excluded, and our mass estimate becomes $0.53^{+0.52}_{-0.35}\ M_{\odot}$.

We have also detected for the first time subtle variations in the spectra of a star undergoing microlensing. Anomalously strong equivalent widths of Hα and TiO were detected while the lens was in transit across the source, an effect that was anticipated because of varying line widths across the face of the star. Given our ability to predict limb crossings in real time, this technique may be used to map out the center-to-limb variations in the spectrum of a future microlensed source.

The results of this paper are attributable to the coordinated efforts of GMAN observers, and are a robust endorsement for microlensing follow-up implemented at 1 m class telescopes.

We would like to thank Antonio Claret for providing limb-darkening coefficients for the MACHO passbands. The authors also wish to thank the skilled GMAN observers at UTSO, Boyd Duffee and Felipe McAuliffe. We are very grateful for the skilled support of the staff and observers at CTIO, in particular Bob Schommer, for flexibility in scheduling GMAN follow-up observations. We thank the NOAO for making nightly use of the CTIO 0.9 m telescope possible.

Astronomy at Wise Observatory is supported by grants from the Israel Science Foundation.

The MOA group thanks the Directors of MJUO and the National Laboratory of High Energy Physics, Japan (KEK) for support, and G. Nankivell and N. Rumsey and staff members of Perth Observatory, MJUO, Camex Ltd., and the Auckland University Science Faculty Workshop for assistance. Grants by Auckland and Victoria Universities, NZ/Japan Foundation, the Ministry of Education, Science, Sports, and Culture of Japan, KEK Laboratory, NZ Lottery Grants Board, the NZ Ministry of Research, Science, and Technology, and the NZ Marsden Fund are gratefully acknowledged.

Work performed at Lawrence Livermore National Laboratory is supported by the Department of Energy (DOE) under contract W7405-ENG-48. Work performed by the Center for Particle Astrophysics personnel is supported in part by the Office of Science and Technology Centers of NSF under cooperative agreement AST 88-09616. Work performed at MSSS0 is supported by the Bilateral Science and Technology Program of the Australian Department of Industry, Technology and Regional Development. W. J. S. is supported by a PPARC Advanced Fellowship. K. G. acknowledges support from DOE Outstanding Junior Investigator, Alfred P. Sloan, and Cottrell awards. C. W. S. thanks the Sloan, Packard, and Seaver Foundations for their generous support.

REFERENCES

Abe, F., et al. 1997, in Proc. 12th IAP Conf., Variable Stars and the Astrophysical Returns of Microlensing Surveys, ed. R. Ferlet & J. P. Maillard (Gif-sur-Yvette: Ed. Frontières), in press
Alard, C., et al. 1995, ESO Messenger, 80, 31
Alard, C., Mao, S., & Guibert, J. 1995, A&A, 300, L17
Alard, C., et al. 1996, ApJ, 458, L17
Albrow, M., et al. 1997, in Proc. 12th IAP Conf., Variable Stars and the Astrophysical Returns of Microlensing Surveys, ed. R. Ferlet & J. P. Maillard (Gif-sur-Yvette: Ed. Frontières), in press
Alcock, C., et al. 1995a, ApJ, 445, 133
———. 1995b, ApJ, 454, L125
———. 1996a, ApJ, 463, L67
———. 1997, ApJ, 479, 119
———. 1998, ApJ, in press
———. 1996d, IAU Circ. 6361
———. 1997, ApJ, 474, 217
Alloin, D. M., & Bica, E. 1989, A&A, 217, 57
Ansari, R., et al. 1996, A&A, 314, 94
———. 1997, A&A, 324, 843
Barbuy, B., Castro, S., Ortolani, S., & Bica, E. 1992, A&A, 259, 607
Benetti, S., Pasquini, L., & West, R. M. 1995, A&A, 294, L37
Bennett, D. P., et al. 1997, ASP Conf. Series 119, ed. D. R. Soderblom (San Francisco: ASP), 95
———. 1996b, Nucl. Phys. B (Proc. Suppl.), 51, 152
Bennett, D. P., & Rhie, S. H. 1996, ApJ, 472, 660
Bessell, M. S., Castelli, F., & Plez, B. 1997, preprint
Bessell, M. S., & Wood, P. R. 1984, PASP, 96, 247
Binney, J. J., Gehrard, O. E., & Spergel, D. 1997, MNRAS, 288, 365
Bono, G., Caputo, F., Castellani, V., & Marconi, M. 1997, A&AS, 121, 327
Claret, A., Díaz-Cordoveś, J., & Giménez, A. 1995, A&AS, 114, 247
Crotts, A. P. S., & Tomaney, A. B. 1996, ApJ, 473, L87
Diaz, A., Terlevich, E., & Terlevich, R. 1989, MNRAS, 239, 325
Díaz-Cordovés, J., Claret, A., & Giménez, A. 1995, A&AS, 110, 329
Dyck, H. M., Benson, J. A., van Belle, G. T., & Ridgway, S. T. 1996, AJ, 111, 1705
Erdelyi-Mendez, M., & Barbuy, B. 1991, A&A, 241, 176
Feast, M. W. 1996, MNRAS, 278, 11
Frogel, J. A., & Whitford, A. E. 1987, ApJ, 320, 199
Frogel, J. A., Persson, S. E., & Cohen, J. G. 1981, ApJ, 246, 842
Gould, A. 1994, ApJ, 421, L71
———. 1996, PASP, 108, 465
———. 1997, ApJ, 483, 98
Gould, A., & Loeb, A. 1992, ApJ, 396, 104
Gould, A., & Welch, D. L. 1996, ApJ, 464, 212
Gray, D. F. 1992, The Observation and Analysis of Stellar Photospheres (Cambridge: Cambridge Univ. Press)
Griest, K., et al. 1991, ApJ, 372, L79
Guarnieri, D., et al. 1996, in Science with the HST II, ed. P. Benvenutti, D. Macchetto, & E. Schreier (Baltimore: STScI), 338
Han, C., & Gould, A. 1995, ApJ, 447, 53
———. 1996, ApJ, 467, 540
Holtzman, J., et al. 1993, AJ, 106, 1826
Humphreys, R. M., & Graham, J. A. 1986, AJ, 91, 522
Ibata, R., Gilmore, G., & Irwin, M. J. 1995, Nature, 370, 194
James, F. 1994, CERN Program Library Long Writeup, D506
Jones, J. E., Alloin, D. M., & Jones, B. T. 1984, ApJ, 283, 457
Jorgensen, U. G., Carlsson, M., & Johnson, H. R. 1992, A&A, 254, 258
Kiraga, M., & Paczyński, B. 1994, ApJ, 430, L101
Kirkpatrick, J. D., Henry, T. J., & McCarthy, D. W. 1991, ApJS, 77, 417
Lang, K. R. 1992, Astrophysical Data (New York: Springer)
Lennon, D. J., et al. 1996, ApJ, 471, L23
Loeb, A., & Sasselov, D. 1995, ApJ, 449, L33
Mao, S., & Paczyński, B. 1991, ApJ, 374, L37
Maoz, D., & Gould, A. 1994, ApJ, 425, L67
Minniti, D. 1996, ApJ, 459, 579
Minniti, D., Liebert, J. W., Olszewski, E. W., & White, S. D. M. 1996, AJ, 112, 590
Nemiroff, R. J., & Wickramasinghe, W. A. D. T. 1994, ApJ, 424, L21
Ortolani, S., Barbuy, B., & Bica, E. 1990, A&A, 236, 362
Paczyński, B. 1991, ApJ, 371, L63
———. 1996, ARA&A, 34, 419
Paczyński, B., et al. 1995, BAAS, 187, 14.07
Peng, E. W. 1997, ApJ, 475, 43
Pratt, M. R., et al. 1996, in IAU Symp. 173, Astrophysical Applications of Gravitational Lensing, ed. C. S. Kochanek & J. N. Hewitt (Dordrecht: Kluwer), 221

Rieke, G., & Lebofski, M. 1985, ApJ, 288, 618
Sasselov, D. 1997, in IAP Colloq. Variable Stars and the Astrophysical Returns of Microlensing Surveys, ed. R. Ferlet, in press
Stetson, P. B. 1994, Daophot II User's Manual
———. 1994b, PASP, 106, 250
Turnshek, D. E., Turnshek, D. A., Craine, E. R., & Boesjaar, P. C. 1985, An Atlas of Digital Spectra of Cool Stars (Tucson: Western Research Co.)
Udalski, A., Szymański, M., Kałużny, J., Kubiak, M., Krzemiński, W., Mateo, M., Preston, G. W., & Paczyński, B. 1994a, Acta Astron., 44, 165
Udalski, A., Szymański, M., Mao, S., Di Stefano, R., Kałużny, J., Kubiak, M., Mateo, M., & Krzemiński, W. 1994b, ApJ, 436, L103
Valls-Gabaud, D. 1994, in Large Scale Structure in the Universe, ed. J. P. Mücket et al. (Singapore: World Scientific), 326
Witt, H. J., & Mao, S. 1994, ApJ, 430, 505
Zhao, H., Rich, R. M., & Spergel, D. N. 1996, MNRAS, 282, 175